Earth and Planetary Science Letters 562 (2021) 116819

Contents lists available at ScienceDirect

Earth and Planetary Science Letters

www.elsevier.com/locate/epsl

Earthquake collapse mechanisms and periodic, migrating seismicity during the 2018 summit collapse at Kīlauea caldera

Celso R. Alvizuri [a,*], Robin S. Matoza [b], Paul G. Okubo [c]

[a] Institute of Earth Sciences, University of Lausanne, Switzerland
[b] Department of Earth Science and Earth Research Institute, University of California, Santa Barbara, United States of America
[c] Department of Earth Sciences, University of Hawai'i at Manoa, Honolulu, Hawai'i, United States of America

ARTICLE INFO

Article history:
Received 12 September 2020
Received in revised form 9 February 2021
Accepted 10 February 2021
Available online 25 February 2021
Editor: H. Thybo

Keywords:
seismic moment tensors
non-double-couple
isotropic
seismicity
caldera collapse
Kilauea volcano

ABSTRACT

The 2018 Lower East Rift Zone eruption of Kīlauea volcano was accompanied by a remarkable and periodic succession of collapses in the summit region. Between May-August the eruption and collapse sequence included 54 earthquakes (M∼5; M5s) observed worldwide, and over 45,000 intervening earthquakes (M≥0). We estimated seismic full moment tensors for the M5s and analyzed the spatio-temporal evolution of the intervening seismicity. The hypocenters were concentrated between 0-3 km depths and reveal arcuate bands that migrated outward by ∼300 m (map view) and downward by ∼200 m. The temporal evolution reveals almost daily successions of escalating earthquake swarms, followed by an M5, followed by a quiescent period. The moment tensors reveal consistent collapse mechanisms with vertical P-axis orientations. Poisson's ratios estimated from the moment tensors were variable at first ($\nu = 0.1 - 0.3$) and from June 26 onward converged to $\nu \sim 0.28$, similar to loading cycles observed in lab experiments. The shallower collapses approximately follow the expanding contour of the crater, while deeper collapses aggregate first to the north of the previous crater and later to the east and south. We interpret that the magma storage complex beneath the summit region comprises a distributed plexus of cracks that progressively evacuated and underwent collapse as magma drained from the summit region to feed the eruption.

1. Introduction

On 2018 Kīlauea volcano experienced its largest flank eruption in 200 years and a dramatic collapse of its caldera. The eruption sequence included the largest earthquake on the island in 43 years (magnitude M6.9; 2018-05-04), 56 other large earthquakes (M∼5) observed worldwide, and over 70,000 earthquakes (M≥0) across the island. In total 54 of the M∼5 events (M5s) occurred in the Kīlauea summit region and were concentrated between 0−3 km depths.

According to Neal et al. (2019), the 2018 flank eruption and caldera collapse at Kīlauea are characterized by inflationary ground deformation starting mid-March, rising lava lake levels at Pu'u 'Ō'ō and Halema'uma'u craters through April, propagating seismicity and lava fountaining towards the Lower East Rift Zone (LERZ). On May 1 the Kīlauea summit region began to deflate and lava lake levels in Halema'uma'u began to drop; on May 4 the M6.9 earthquake occurred at about 6 km beneath Kīlauea's south flank. Soon after the M6.9 earthquake, deflation of Kīlauea's summit accelerated, and by May 10 the lava lake level had dropped by more than 300 m. Toward the end of May, the summit began to subside in episodic, almost daily patterns, with the crater floor dropping by several meters during each episode. These patterns are characterized by escalating earthquake swarms of up to 700 events per day, each followed by an M5 and a short period of nominal seismicity levels. The last collapse event occurred on August 2, at about the same time as lava effusion stopped at the LERZ.

The 2018 activity at Kīlauea prompted major field sampling and enhanced monitoring by the USGS Hawaiian Volcano Observatory and collaborators which, along with continuously operated networks, offer unprecedented capabilities to observe and interpret sustained eruption and caldera collapse in Hawai'i. Since 1900 only six other caldera collapses have been documented in detail (Gudmundsson et al., 2016), and seismological studies of caldera collapses include: Piton de la Fournaise, Réunion Island (2007) (Michon et al., 2007), Miyakejima, Japan (2000) (Geshi et al., 2002; Minson et al., 2007; Shuler et al., 2013b), Bárdarbunga, Iceland

* Corresponding author.
E-mail address: celso.alvizuri@unil.ch (C.R. Alvizuri).

https://doi.org/10.1016/j.epsl.2021.116819

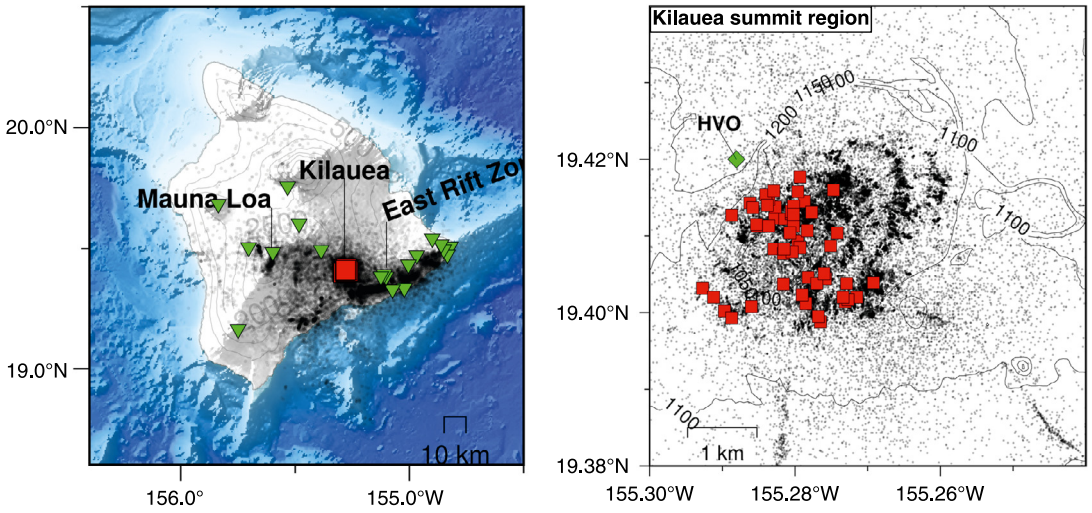

Fig. 1. Seismicity in the Island of Hawai'i and in the Kīlauea summit region during 2018. Most of the seismicity was generated during the eruption at the Lower East Rift Zone and during the summit collapse at Kīlauea caldera (over 70,000 events; M≥0). We focus on the 54 major seismic events (red squares; M≥5) and intervening seismicity which occurred near Halema'uma'u pit crater in the Kīlauea summit region. We estimated seismic full moment tensors for the 54 events (M5s) using broadband waveform data from stations on the island (green triangles), and analyzed the spatial and temporal distribution of the intervening seismicity. (For interpretation of the colors in the figure(s), the reader is referred to the web version of this article.)

(2014-2015) (Gudmundsson et al., 2016), and Fernandina, Galápagos Islands (1968) (Simkin and Howard, 1970).

In this study, we analyze the collapse events in the Kīlauea summit region; we estimate seismic source mechanisms for the 54 M5s by computing their seismic full moment tensors using waveform data, and analyze spatiotemporal variations in the intervening seismicity using a comprehensive catalog of recently relocated hypocenters for the region. Our results reveal remarkably consistent and episodic collapse mechanisms, with episodic and migrating seismicity.

2. Data and methods

We estimated seismic moment tensors for the M5s using waveforms from all possible broadband seismic stations within a 2,000 km radius, available from IRIS-DMC, and hypocenters from a comprehensive catalog of relocated seismicity (Matoza et al., 2021). The waveforms were downloaded and processed using ObsPy, a python-based package for seismology (e.g., Krischer et al., 2015).

The processing steps for each event were: (1) obtain three-component waveforms and metadata from IRIS-DMC; (2) remove instrument response using an 4-pole Butterworth filter with corner frequencies 0.005, 0.006, 10.0, and 15.0 Hz (flat bandpass 0.006–10.0 Hz); (3) using the source-station azimuth and the sensor orientation angle, rotate horizontal components to radial and transverse directions. Additional processing steps, such as cutting time windows and additional bandpass filtering were applied during the moment tensor inversions. In our analysis, the waveforms at near stations (up to ∼15 km distance) show larger amplitude oscillations that may be related to near field effects, while farther stations (>100 km) show waveforms with lower signal-to-noise ratio. Therefore, for our moment tensor estimates we used data from stations within 15–100 km distances (Fig. 1).

We estimate full seismic moment tensors and their uncertainties for each event using the methodology described in Alvizuri et al. (2018). The method involves performing an efficient search over the full parameter space of moment tensors (lune longitude, lune latitude, strike, dip, and rake) including magnitude, and uses a geometric parameterization for moment tensors and their uncertainty quantification (for details and other applications, see e.g. Alvizuri and Tape, 2016; Silwal and Tape, 2016; Alvizuri et al., 2018). For each moment tensor in the parameter space, synthetic seismograms are computed using a frequency-wavenumber approach (Zhu and Rivera, 2002) with a 1D (layered) Earth model, then the seismograms are compared with observed waveforms via a misfit function. The synthetic seismograms for this study were computed using a 1D layered model for the region obtained from CRUST1.0 (Laske et al., 2013).

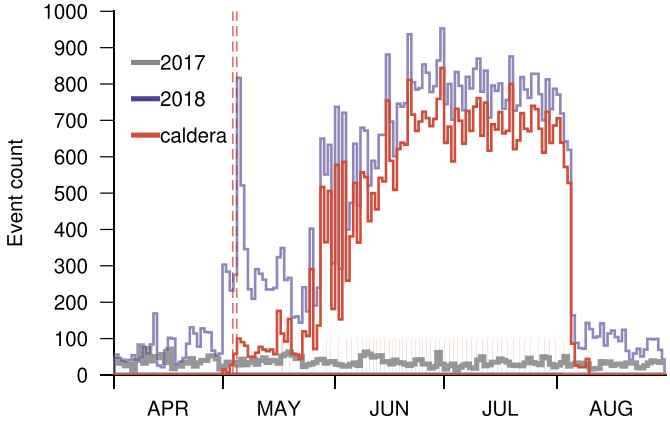

Fig. 2. Seismicity levels in the Island of Hawai'i (blue) and in the Kīlauea summit region (red) during 2018 (the gray line shows reference seismicity levels during 2017). The daily seismicity at Kīlauea increased twice in May (red dashed lines) from background levels of ∼30 events per day, to ∼300/day on 1 May 2018, and again to ∼800/day following the Mw 6.9 earthquake on 2018-05-04. The M5s (red short lines) and intervening seismicity occurred in succession between May-August.

The moment tensor methodology has proven useful for earthquake source characterization for a range of settings in the Earth, including Uturuncu volcano in southwest Bolivia (Alvizuri and Tape, 2016); tectonic events at a subduction zone in southcentral Alaska (Alvizuri et al., 2018); events possibly related to metamorphism in the Himalaya lower crust (Alvizuri and Hetényi, 2019); and nuclear tests and cavity collapses in western USA and in North Korea (Alvizuri et al., 2018; Alvizuri and Tape, 2018).

We complemented our moment tensor results by analyzing the temporal and spatial distribution of hypocenters at Kīlauea volcano for 2018. The hypocenters are from a recent comprehensive study which relocated seismicity from 32 years (1986-2018) for the Island of Hawai'i (Matoza et al., 2021). Their relocations were done with the GrowClust algorithm (Trugman and Shearer, 2017) which

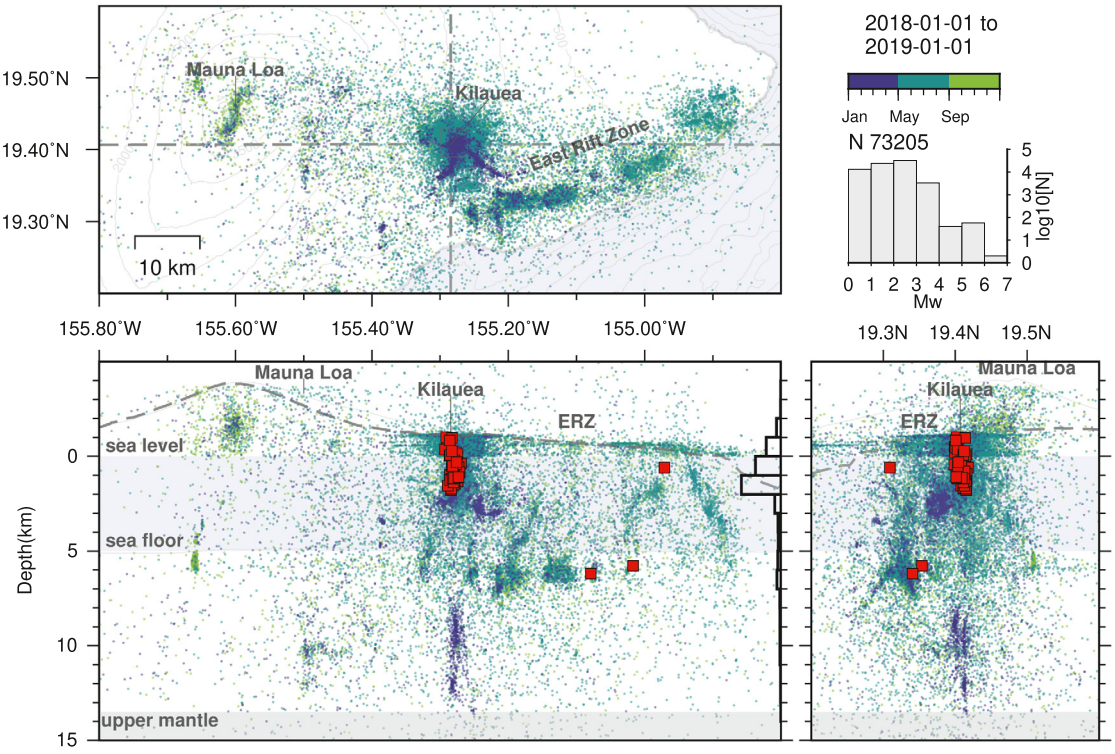

Fig. 3. The M5s and seismicity in the southeast portion of the island during 2018. The seismicity (colored by time) until May was concentrated beneath the Kīlauea summit region at depths 2-4 km and 7-13 km (bsl); it was followed by elevated seismicity in the summit region and the Lower East Rift Zone; then followed by the M5s and their intervening seismicity until August when seismic activity suddenly decreased to background levels. (Vertical exaggeration is 3X; the crosshairs are centered at Halema'uma'u pit crater.)

combines waveform cross-correlation, hierarchical cluster analysis and relative relocations; for details, see Matoza et al. (2013, 2021). We focused on the seismicity near Halema'uma'u pit crater in the Kīlauea summit region between longitudes [-155.30, -155.24], latitudes [19.38, 19.44], and depths [0, 3] km (Fig. 1). In total, 54 M5s occurred between May-August in the summit region.

3. Results

3.1. Seismicity

The seismicity at Kīlauea shows three main periods during 2018 (Fig. 2): (1) January-April, seismic activity at background levels of about 30 events per day; (2) May-August, activity changes suddenly to 300/day and again to sustained levels up to 800/day; (3) August 4-December, activity returns to background levels. Fig. 3 shows hypocenters on map and cross sections for the three periods above.

During the first period (Jan-May) the seismicity was concentrated beneath the summit region and was typical for the region (with approximately the same distribution from 1986-2017). The seismicity occurred from the surface to about 3 km below sea level (bsl) and from 7-13 km bsl, and in the upper West and upper East Rift Zones from 1-3 km bsl. The gap between ~3-7 km is attributed to the relatively aseismic magma storage reservoir. The next period (May-Aug) shows elevated seismicity in the summit region and along ERZ (depths 3-7 km bsl). In the next period (Aug-Dec) the seismic activity decreased to background levels (though slightly more elevated than 2017 levels), and increased beneath Mauna Loa summit.

Fig. 4 shows a closer view of the seismicity in the summit region during May-August (panels a-d). Seismic activity in May increases and is generally diffuse, then changes into distinct arcuate bands throughout June-July, then changes back into diffuse in August until it suddenly drops to background levels on 3 August.

During this period the hypocenters migrated radially outward (map view; epicentral distances with respect to reference location $(-155.285, 19.420)$) and downward (cross-section view); Fig. 5 shows hypocentral depths with time beneath the Kīlauea summit region for 2018. This result shows that the peaks in seismicity are concentrated between depths 0.5-2 km beneath the summit, and throughout June-July they migrate about 200 m downward and 300 m radially outward.

3.2. Seismic moment tensors

In our results the synthetic seismograms show good agreement with the observations. The moment tensor uncertainty estimates for each event show best fitting mechanisms that are localized toward the negative isotropic (−ISO) region on the lune; for details on the uncertainty analysis, see Alvizuri et al. (2018). The supplement shows the best-fitting mechanisms for the 54 events analyzed here, their waveform fits and uncertainty estimates.

The best-fitting moment tensors for the 54 M5s show consistent mechanisms with their P-axes oriented vertically and magnitudes between M4.9–5.6 (Table S2). The source durations for the first 5/54 events require source durations that decrease from 20 to 5 seconds, while the remaining 49/54 events range between 1-2 seconds (Table S2). Fig. 6 shows three periods of elevation models for the summit region, together with the M5s, their shifting epicenters, and their moment tensor beachballs.

The seismic moment tensor $\mathbf{M}$ is a 3×3 mathematical matrix that represents the seismic source and can be related with a single-process source model as $M_{ij} = \mu\left(n_i s_j + n_j s_i\right) + \lambda\,\delta_{ij}\,\mathbf{S}\cdot\mathbf{N}$ (Aki and Richards, 1980), and Poisson's ratio $\nu = \lambda/2(\lambda + \mu)$. In

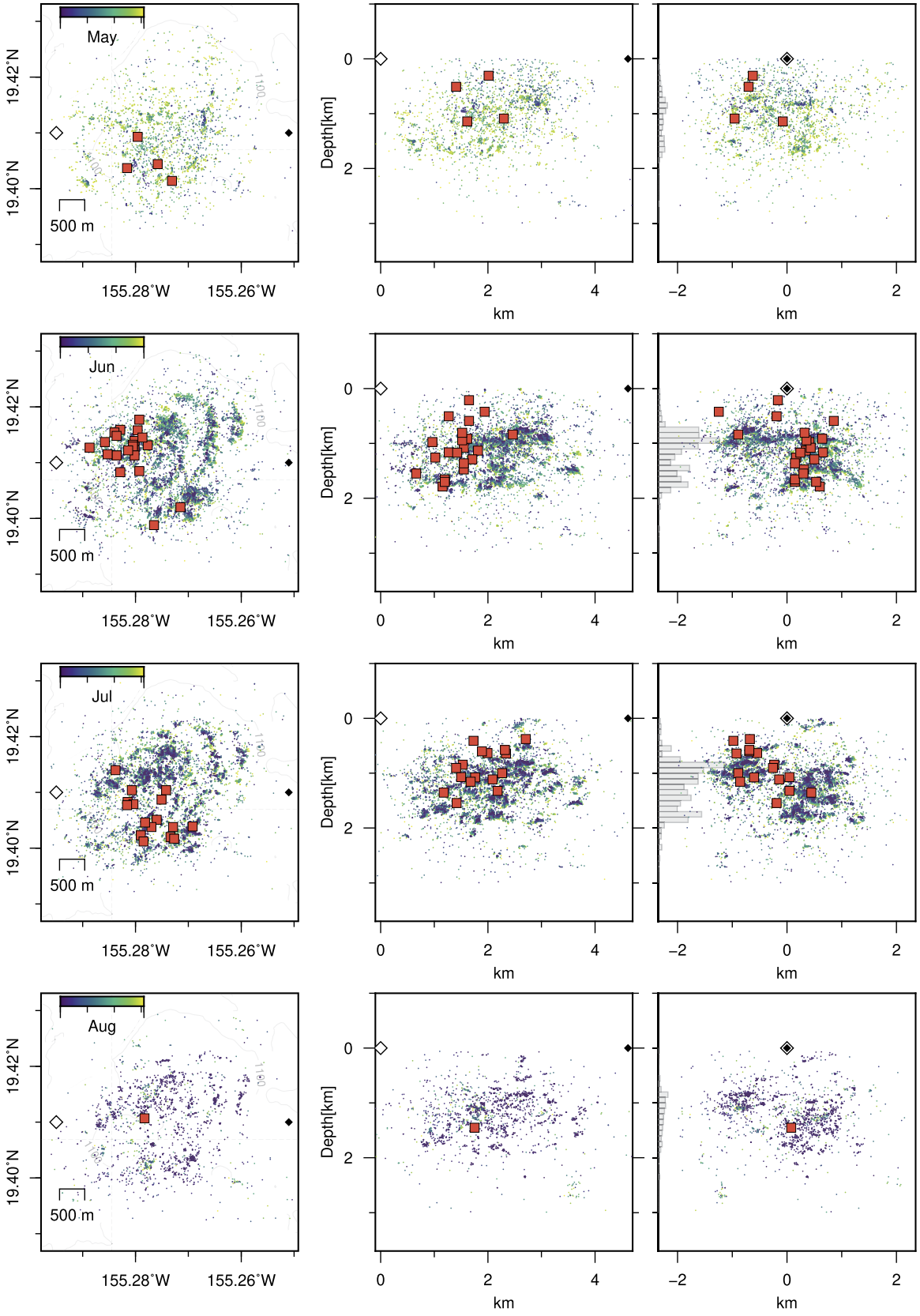

Fig. 4. The M5s and intervening seismicity in the Kīlauea summit region from May-August, 2018. Each row shows one month of hypocenters (top row is for May, bottom row is for August). The left column shows map views; the center and right columns show cross-sections looking toward north and toward west. The M5s cluster to the north of Halema'uma'u crater (cross-hairs) in June, and to the east and southeast of the crater in July. The seismicity in map view forms into arcuate bands to the northeast of Halema'uma'u, which become prominent in June-July. During these months the seismicity migrated downward (cross-section view) and radially outward (map view).

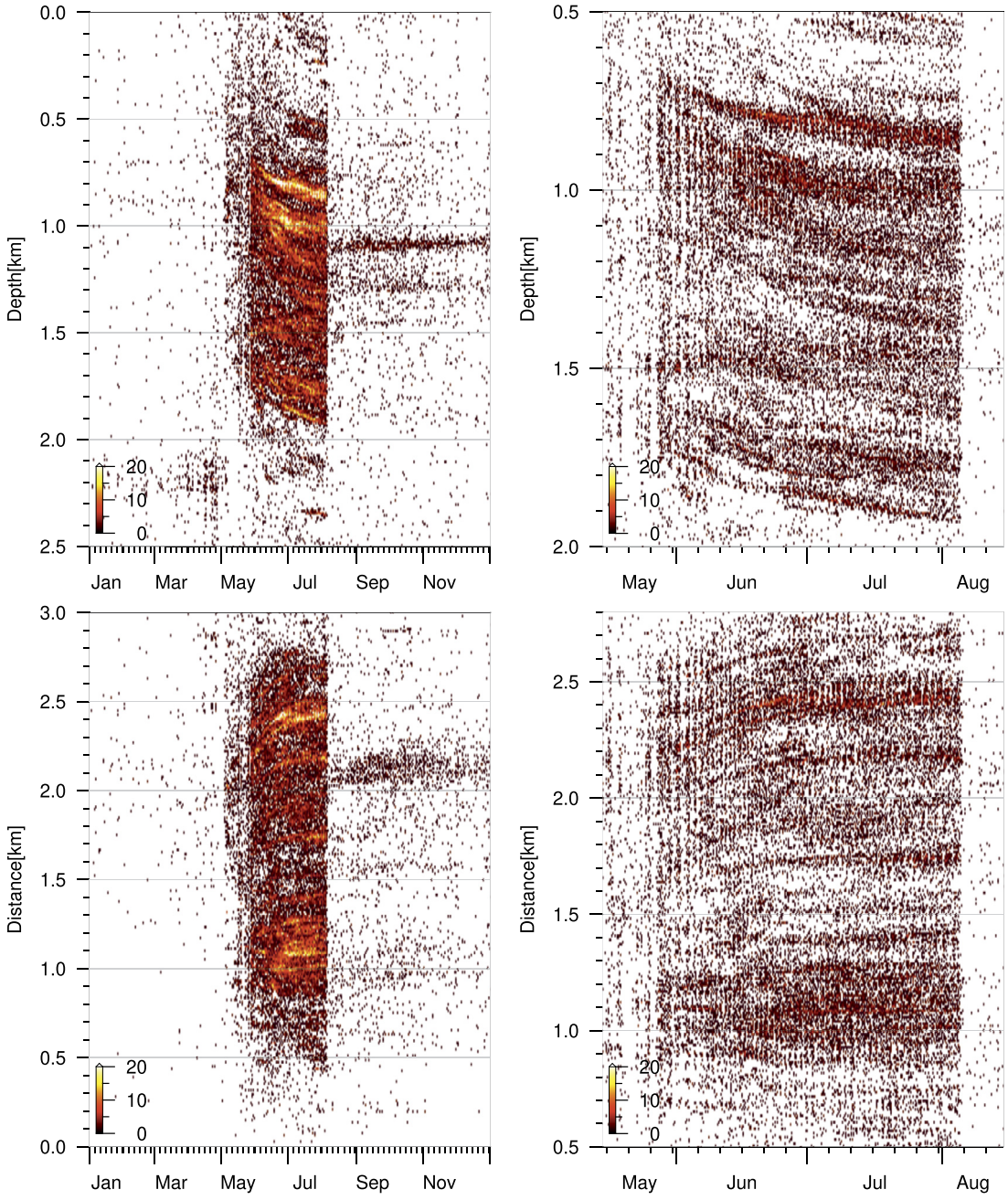

Fig. 5. Between May-August the hypocenters in the Kīlauea summit region migrated downward by about 200 m (top panels) and radially outward by about 300 m (bottom panels). The heatmaps were computed using hypocenters within the same boundaries as in Fig. 4, at 1-day bins and 10-meter depth intervals. The radial distances were computed from reference location (−155.285, 19.420), north of Halema'uma'u crater.

this model the seismic source **M** represents (possibly oblique) slip on a planar fault, and is characterized by the Lamé elastic parameters (λ, μ), and an angle α between normal **N** and slip **S** vectors. For details, see Dufumier and Rivera (1997); Tape and Tape (2013); and for applications in other settings in the Earth's crust, see e.g. Alvizuri and Tape (2016); Alvizuri and Hetényi (2019).

We computed Poisson's ratio ν from the 54 events at Kīlauea and analyzed their evolution. For the events up to June 25 their Poisson's ratios range between $\nu = 0.1 - 0.3$; from June 26-on they converge to values near $\nu = 0.28$. Fig. 7 summarizes these results and other observations with time: (a) moment tensor focal mechanisms and accompanying seismicity; (b) median seismic moment and times of the M5s, tilt from station UWD (north component) near the northwest caldera rim; (c) time difference between consecutive events and Poisson's ratios estimated from the moment tensors.

4. Discussion

4.1. Moment tensors and collapse mechanisms

Seismic moment tensor studies for nuclear explosions at the Nevada Test Site (NTS; USA) and Punggye-Ri (North Korea) reveal mechanisms with +ISO parameters for the explosions; and secondary events following some explosions show −ISO parameters and are presumed cavity collapses (e.g., Ford et al., 2009; Chiang et al., 2014; Cesca et al., 2017; Alvizuri et al., 2018; Alvizuri and Tape, 2018).

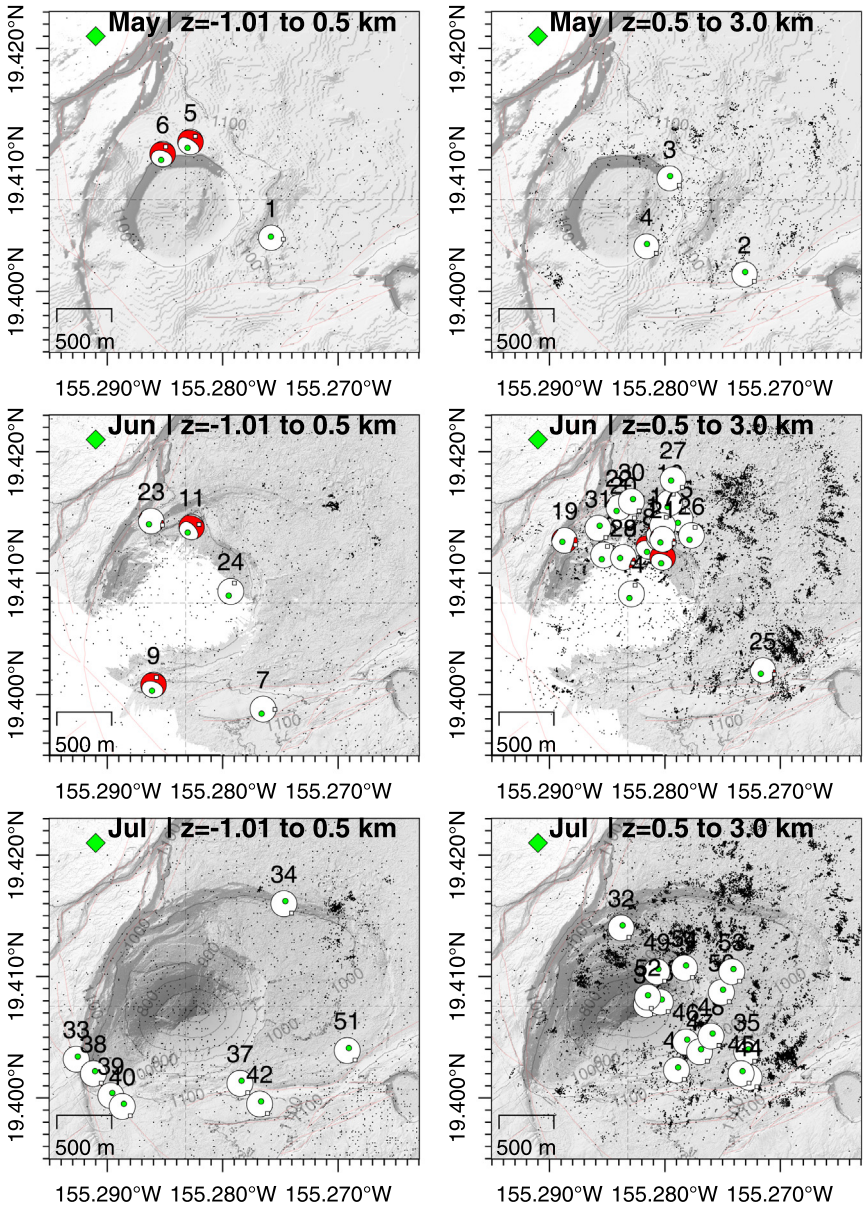

Fig. 6. The M5s and their focal mechanisms (beachballs) between May-July, at two depth slices. The shallower M5s (depths −1 to 0.5 km bsl) approximately follow the expanding crater rim; while the deeper M5s cluster to the north of the previous crater (June), and to the east and southeast (July). Green circles denote the beachball P axes, which appear vertically oriented. The background elevation model for May is from ETOPO1, and for June-July from two LiDAR campaigns by the USGS. The green diamond shows tiltmeter station UWD.

Our moment tensor results for the M5s at Kīlauea reveal consistent mechanisms that converge toward −ISO, with vertical P-axes orientations, and with source durations that decrease from ∼20 to 5 seconds and converge to ∼2 seconds from May 30-onwards (Figs. 6–8). Similar mechanisms were also observed from the caldera collapse at Miyakejima (Shuler et al., 2013a) and Bárdarbunga volcano (Gudmundsson et al., 2016). The moment tensors for Miyakejima show source durations on the order of 50–60 seconds (these were not available for Bárdarbunga), and both settings show mechanisms with vertical P axes (though the analysis for Miyakejima was restricted to deviatoric moment tensors).

Seismic source studies at volcanoes often combine moment tensors with single forces and complex geometries to study various processes such as fluid-rock interaction (Kumagai et al., 2005; Chouet et al., 2010; Matoza et al., 2015), and caldera collapse events (e.g., Kumagai, 2001; Duputel and Rivera, 2019). The events we analyzed for Kīlauea may also arise from combinations of similar processes, though the waveforms in our results show the moment tensor alone adequately fits the observations.

Non-double-couple moment tensors may also arise as artifacts from imperfect Earth models, anisotropy, curved faults, etc. (e.g., Kawasaki and Tanimoto, 1981; Frohlich, 1994; Julian et al., 1998). These are known tradeoffs in full moment tensor estimation, and can also be addressed with multiple force systems, finite source studies (e.g., Fichtner and Tkalčić, 2010), more accurate structure models, etc.

4.2. Collapse mechanisms and deformation

Field studies at NTS (e.g., Houser, 1969; Massé, 1981), at quarry sites (e.g., Scandone, 1990), and analogue sandbox experiments (Acocella, 2007; Ruch et al., 2012) provide insight into the kinematic evolution of caldera collapses from small (cm) to intermediate scales (100s m). They show block-like collapse structures and

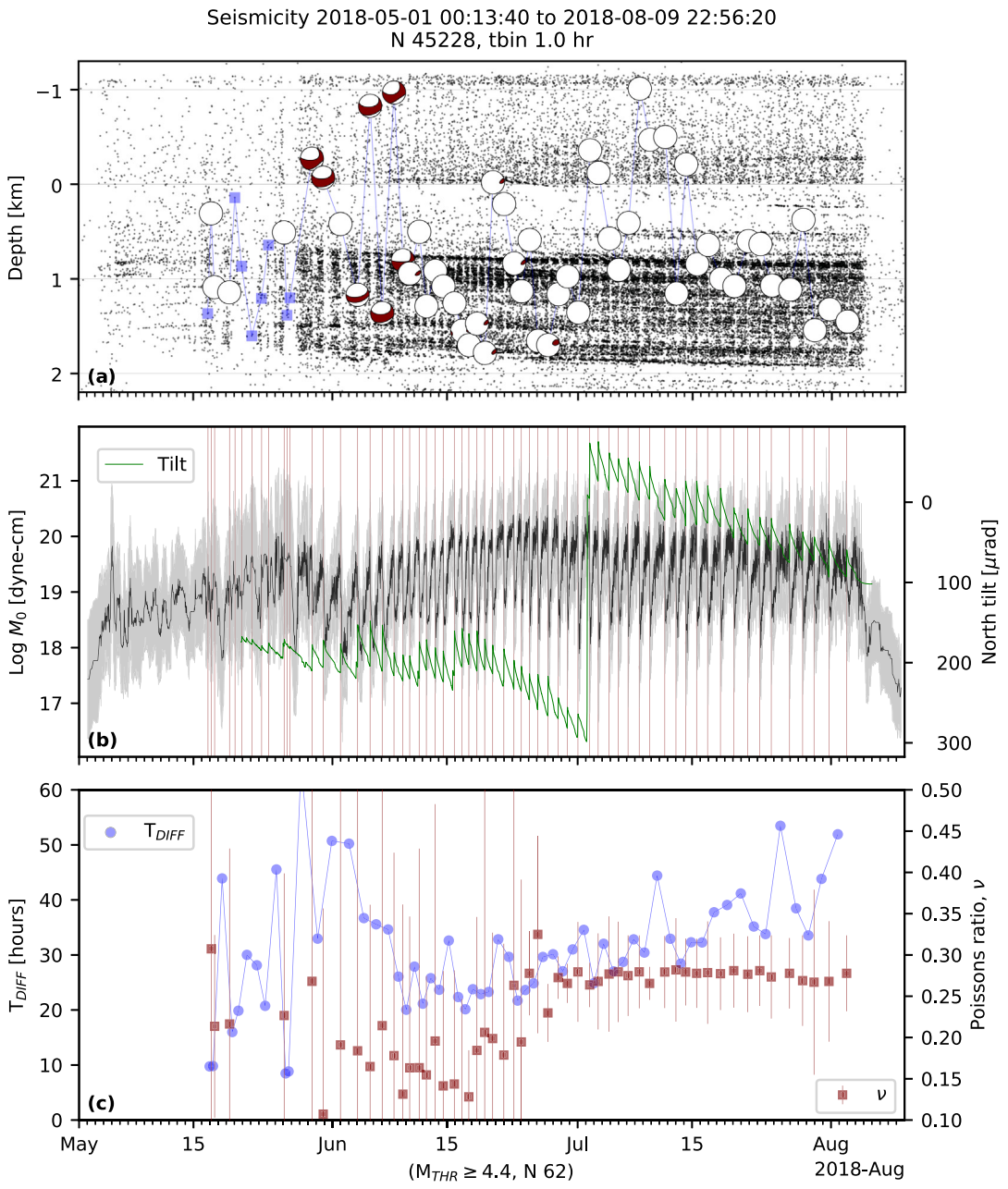

Fig. 7. The M5s and their beachballs, together with intervening seismicity and tiltmeter data in the summit region. (a) Beachballs in cross-section view (cf Fig. 4) and hypocenters; (b) median seismic moment (black lines), mean absolute deviation (gray), times of the large events (red lines), and tiltmeter data (green) for station UWD (north component; the offset is due to recentering of the sensor); (c) time difference (T_{DIFF}; blue circles) between consecutive events ($M_{THR} \geq 4.4$) and Poisson's ratios (red) estimated from the M5s.

fault systems that develop near the surface, with a range of radial and concentric cracks and chimney collapse formations at depth.

In our analysis, the hypocenters in the summit region (including the M5s) were concentrated between 0-3 km depth, and between May-August migrated downward by about 200 m. During this period the summit crater caved downward by up to 500 m while the crater rim expanded by about 1000 m. The epicenters in some areas form arcuate bands and radial streaks (depths 0.5∼2.0 km), and some large, shallower events (0∼1.5 km depths) approximately follow the expanding contours of the crater (Fig. 6).

4.3. Collapse and seismicity cycles

During May-August, the seismicity beneath the summit region shows almost daily cycles of escalating earthquake swarms that end with an M5 and are followed by approximately 1 hr of relatively quiet periods (N≤10; similar patterns were also observed by Shelly and Thelen (2019); Butler (2020)). This style in cyclic seismicity continued until ∼Jun 28, where it changed into more sudden onsets (the supplement shows additional views and shorter time windows).

The seismicity cycles also coincide with tiltmeter observations from station UWD (Fig. 7) to the west of the crater, which shows a long period trend of tilt to the southeast, towards Halema'uma'u and intervening and periodic offsets that coincide with the times of the M5s, and point away from Halema'uma'u. A recent study (Segall et al., 2019) suggests that these trends follow a primarily deflation process (revealed by subsidence at a GPS station at the Halema'uma'u rim) and a secondary process of ash emissions as observed by the radially outward transients (up to 89 μrad at

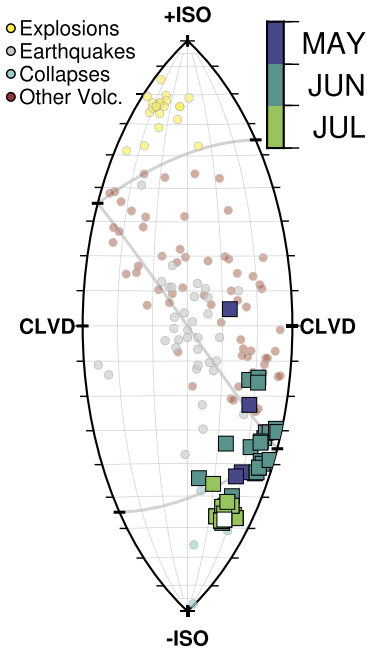

Fig. 8. Lune representation of mechanisms from the M5s and other studies (Alvizuri and Tape, 2016; Alvizuri et al., 2018; Alvizuri and Tape, 2018). The lune provides a window into seismic moment tensors and organizes them into source type regions (e.g. Tape and Tape, 2019). Explosion mechanisms are on top (+ISO); collapses are on the bottom (−ISO); earthquakes are at the center (Figure S1 describes the lune in more detail). The M5s were remarkably consistent: they had similar magnitudes (M∼5); they occurred in orderly, almost daily succession; their mechanisms had similar orientations; and their source types converged towards −ISO and clustered tightly from July-onwards.

UWD). Similar tiltmeter transients were also observed on 2017 at Piton de la Fournaise (PdF), and may reflect a continuum of deformation from the roof of the magma chamber to the surface (Michon et al., 2007, 2009).

The episodic collapses at Kīlauea also appear coupled to pressure changes within the magmatic system. A recent study estimated lava effusion rates at a newly developed fissure in the LERZ using ground-based video and time-lapsed images (Patrick et al., 2019), and they observe dual cycles in lava eruption rates, one with periods of 5–10 minutes where effusion rates change from ∼350–1750 $m^3\,s^{-1}$; another as long-term surges in effusion rates and occurring no later than 20 min after the collapse events, with effusion rates changing from ∼300–500 $m^3\,s^{-1}$ before collapse, up to ∼1400 $m^3\,s^{-1}$ after collapse. This suggests a hydraulic connection where the summit reservoir provides pressurized magma to the flank vents, in turn the flank vents regulate draining at the summit reservoir, and where the summit collapse events induce pressure surges within the magma conduits.

4.4. Controls on times between collapses

The events in the summit region group into two populations, depending on their magnitudes at threshold M_{THR}= 4.4. Similar M_{THR} values were also observed in Miyakejima, Piton de la Fournaise and Fernandina (e.g. Michon et al., 2011, and references there), and suggest similar collapse dynamics.

For the events in the summit region and M<M_{THR}, the time difference between consecutive events T_{DIFF} approaches zero, and suggests the events are not causally linked (e.g., Poisson distributed; Gardner and Knopoff, 1974). For M≥M_{THR}, T_{DIFF} varies between 10–60 hours until June 9, and from June 10–onwards they converge on a trend that increases from about 20–40 hr.

T_{DIFF} together with a piston intrusion model (Kumagai, 2001), relates to frictional difference F_{SD}, piston geometry and mass, and lava effusion rates. These were variable for Kīlauea (e.g., Anderson et al., 2019; Patrick et al., 2019). Nevertheless assuming all other variables constant, then $T_{DIFF} \propto F_{SD}$. In other words, T_{DIFF} is in part controlled by rock mass, frictional difference, magma draining rates, and possibly causally, where one event leads to the next.

4.5. Collapse mechanisms and structure change

The shallow magma reservoir beneath the Kīlauea summit region is estimated to comprise a plexus of sills, dikes, magma filled cracks, and void space (Fiske and Kinoshita, 1969; Dawson et al., 1999; Chouet et al., 2010; Johnson et al., 2010). Towards the end of May the lava lake at Halema‘uma‘u crater was no longer visible, which may indicate partial draining from the magma reservoir.

Core samples down to ∼1,200 m beneath the summit region reveal mainly basalt (Zablocki et al., 1974; Keller et al., 1979), and a seismic tomography study for Kīlauea estimated Poisson's ratios between $\nu = 0.25 - 0.32$ (Dawson et al., 1999). Lab experiments where basalt samples are subjected to cyclic loading show incremental Poisson's ratios after each cycle, up to $\nu = 0.3$ (e.g., Schultz, 1993), and $\nu = 0.5$ for samples from Mt. Etna (Heap et al., 2009).

The Poisson's ratios estimated from the M5s are initially variable ($\nu = 0.3$ to 0.1) and converge ($\nu \sim 0.28$) from June 26-onwards. These changes may reflect similar loading cycles as observed in the lab, including possible material changes, within a setting that becomes progressively consolidated and less accommodating after each successive M5.

Brittle failure associated with structural collapse is consistent with the M5s and broad seismicity features presented here. The pre-collapse Kīlauea summit included, however, a complex magma and hydrothermal system; some of the lower magnitude seismicity within the collapse sequence could be long-period (LP) seismicity associated with magma-water interaction or water flashing to steam as new contacts were made, old structural barriers breached, or pressures released on fluid-filled voids (Chouet and Matoza, 2013, and references there).

Historically, the summit seismicity at Kīlauea includes shallow “LPC-A” events which are observed in abundance accompanying rapid summit deflation, after the onset of fountaining downrift at Pu‘u ‘Ō‘ō vent (Okubo and Nakata, 2003). In our analysis we found that 43/54 of the M5s associate with LPC-A seismicity in the summit, which suggests the LPC-A events possibly share similar collapse mechanisms as the M5s.

5. Conclusion

The 2018 caldera collapse at Kīlauea volcano was accompanied by 54 earthquakes (M∼5; M5s) and intervening seismicity which were concentrated beneath the summit region down to ∼3 km depths. We estimated seismic full moment tensors for the M5s using waveform data from broadband seismic sensors, and analyzed spatiotemporal changes in the intervening seismicity. The M5s and intervening seismicity occurred in remarkable, almost daily succession, in consistent styles, and suggests widely collapsing material.

The shallow M5s follow approximately the contours of the expanding crater and appear related to the collapsing structures observed from aerial views. The deeper M5s are concentrated between north and southeast of Halema‘uma‘u pit crater. The moment tensors reveal consistent mechanisms with negative isotropic parameters suggesting predominant material collapses, similar to chimney collapses observed in analogue experiments and at nuclear explosion sites.

Poisson's ratios estimated from the moment tensors are initially variable ($\nu = 0.1 - 0.3$) and converge ($\nu \sim 0.28$) from June 26-

onwards. These changes may reflect loading cycles and material changes as observed in lab experiments, and may reflect consolidating material after each successive M5.

The intervening seismicity forms into arcuate bands (map view) also east and northeast of the crater; it migrated downward by ∼200 m and radially outward (map view) by ∼300 m; and shares similar mechanisms as the M5 collapses which suggests a widely collapsing plexus. Further work estimating source mechanisms for lower magnitude seismicity may confirm these results.

Declaration of competing interest

The authors declare that they have no known competing financial interests or personal relationships that could have appeared to influence the work reported in this paper.

Acknowledgements

We thank Joël Ruch for illuminating discussions about faulting and collapse styles at Kīlauea and other calderas, and Carl Tape & Walter Tape for discussion about moment tensors. We thank the editor Dr. Hans Thybo and two anonymous reviewers whose comments helped to improve our manuscript. R.S.M. was supported by NSF grant EAR-1446543.

Appendix A. Supplementary material

Supplementary material related to this article can be found online at https://doi.org/10.1016/j.epsl.2021.116819.

References

Acocella, V., 2007. Understanding caldera structure and development: an overview of analogue models compared to natural calderas. Earth-Sci. Rev. 85, 125–160. https://doi.org/10.1016/j.earscirev.2007.08.004.

Aki, K., Richards, P.G., 1980. Quantitative Seismology, Theory and Methods. W. H. Freeman, San Francisco, Calif., USA.

Alvizuri, C., Hetényi, G., 2019. Source mechanism of a lower crust earthquake beneath the Himalayas and its possible relation to metamorphism. Tectonophysics 769, 128153. https://doi.org/10.1016/j.tecto.2019.06.023.

Alvizuri, C., Silwal, V., Krischer, L., Tape, C., 2018. Estimation of full moment tensors, including uncertainties, for nuclear explosions, volcanic events, and earthquakes. J. Geophys. Res., Solid Earth 123, 5099–5119. https://doi.org/10.1029/2017JB015325.

Alvizuri, C., Tape, C., 2016. Full moment tensors for small events ($M_w < 3$) at Uturuncu volcano, Bolivia. Geophys. J. Int. 206, 1761–1783. https://doi.org/10.1093/gji/ggw247.

Alvizuri, C., Tape, C., 2018. Full moment tensor analysis of nuclear explosions in North Korea. Seismol. Res. Lett. 89, 2139–2151. https://doi.org/10.1785/0220180158.

Anderson, K.R., Johanson, I.A., Patrick, M.R., Gu, M., Poland, P.S.M.P., Montgomery-Brown, E.K., Miklius, A., 2019. Magma reservoir failure and the onset of caldera collapse at Kīlauea Volcano in 2018. Science 366, eaaz1822. https://doi.org/10.1126/science.aaz1822.

Butler, R., 2020. Volcanic earthquake foreshocks during the 2018 collapse of Kīlauea Caldera. Geophys. J. Int. 220, 71–78. https://doi.org/10.1093/gji/ggz425.

Cesca, S., Heimann, S., Kriegerowski, M., Saul, J., Dahm, T., 2017. Moment tensor inversion for nuclear explosions: what can we learn from the 6 January and 9 September 2016 nuclear tests, North Korea? Seismol. Res. Lett. 88, 300–310. https://doi.org/10.1785/0220160139.

Chiang, A., Dreger, D.S., Ford, S.R., Walter, W.R., 2014. Source characterization of underground explosions from combined regional moment tensor and first-motion analysis. Bull. Seismol. Soc. Am. 104, 1587–1600. https://doi.org/10.1785/0120130228.

Chouet, B.A., Dawson, P.B., James, M.R., Lane, S.J., 2010. Seismic source mechanism of degassing bursts at Kilauea Volcano, Hawaii: results from waveform inversion in the 10–50 s band. J. Geophys. Res., Solid Earth 115, B09311. https://doi.org/10.1029/2009JB006661. 00056.

Chouet, B.A., Matoza, R.S., 2013. A multi-decadal view of seismic methods for detecting precursors of magma movement and eruption. J. Volcanol. Geotherm. Res. 252, 108–175. https://doi.org/10.1016/j.jvolgeores.2012.11.013.

Dawson, P.B., Chouet, B.A., Okubo, P.G., Villaseñor, A., Benz, H.M., 1999. Three-dimensional velocity structure of the Kilauea Caldera, Hawaii. Geophys. Res. Lett. 26, 2805–2808. https://doi.org/10.1029/1999GL005379.

Dufumier, H., Rivera, L., 1997. On the resolution of the isotropic component in moment tensor inversion. Geophys. J. Int. 131, 595–606.

Duputel, Z., Rivera, L., 2019. The 2007 caldera collapse of Piton de la Fournaise volcano: source process from very-long-period seismic signals. Earth Planet. Sci. Lett. 527, 115786. https://doi.org/10.1016/j.epsl.2019.115786.

Fichtner, A., Tkalčić, H., 2010. Insights into the kinematics of a volcanic caldera drop: probabilistic finite-source inversion of the 1996 Bárdarbunga, Iceland, earthquake. Earth Planet. Sci. Lett. 297, 607–615. https://doi.org/10.1016/j.epsl.2010.07.013.

Fiske, R.S., Kinoshita, W.T., 1969. Inflation of Kilauea volcano prior to its 1967-1968 eruption. Science 165, 341–349.

Ford, S.R., Dreger, D.S., Walter, W.R., 2009. Identifying isotropic events using a regional moment tensor inversion. J. Geophys. Res. 114. https://doi.org/10.1029/2008JB005743.

Frohlich, C., 1994. Earthquakes with non-double-couple mechanisms. Science 264, 804–809.

Gardner, J.K., Knopoff, L., 1974. Is the sequence of earthquakes in Southern California, with aftershocks removed, Poissonian?. Bull. Seismol. Soc. Am. 64, 1363–1367.

Geshi, N., Shimano, T., Chiba, T., Nakada, S., 2002. Caldera collapse during the 2000 eruption of Miyakejima Volcano, Japan. Bull. Volcanol. 64, 55–68. https://doi.org/10.1007/s00445-001-0184-z.

Gudmundsson, M.T., Jónsdóttir, K., Hooper, A., Holohan, E.P., Halldórsson, S.A., Ófeigsson, B.G., Cesca, S., Vogfjörd, K.S., Sigmundsson, F., Högnadóttir, T., Einarsson, P., Sigmarsson, O., Jarosch, A.H., Jónasson, K., Magnússon, E., Hreinsdóttir, S., Bagnardi, M., Parks, M.M., Hjörleifsdóttir, V., Pálsson, F., Walter, T.R., Schöpfer, M.P.J., Heimann, S., Reynolds, H.I., Dumont, S., Bali, E., Gudfinnsson, G.H., Dahm, T., Roberts, M.J., Hensch, M., Belart, J.M.C., Spaans, K., Jakobsson, S., Gudmundsson, G.B., Fridriksdóttir, H.M., Drouin, V., Dürig, T., Aðalgeirsdóttir, G., Riishuus, M.S., Pedersen, G.B.M., van Boeckel, T., Oddsson, B., Pfeffer, M.A., Barsotti, S., Bergsson, B., Donovan, A., Burton, M.R., Aiuppa, A., 2016. Gradual caldera collapse at Bárdarbunga volcano, Iceland, regulated by lateral magma outflow. Science 353, aaf8988. https://doi.org/10.1126/science.aaf8988.

Heap, M.J., Vinciguerra, S., Meredith, P.G., 2009. The evolution of elastic moduli with increasing crack damage during cyclic stressing of a basalt from Mt. Etna volcano. Tectonophysics 471, 153–160. https://doi.org/10.1016/j.tecto.2008.10.004.

Houser, F., 1969. Subsidence related to underground nuclear explosions, Nevada Test Site. Bull. Seismol. Soc. Am. 59, 2231–2251.

Johnson, D.J., Eggers, A.A., Bagnardi, M., Battaglia, M., Poland, M.P., Miklius, A., 2010. Shallow magma accumulation at Kīlauea Volcano, Hawai'i, revealed by microgravity surveys. Geology 38, 1139–1142. https://doi.org/10.1130/G31323.1.

Julian, B.R., Miller, A.D., Foulger, G.R., 1998. Non-double-couple earthquakes: 1. Theory. Rev. Geophys. 36, 525–549. https://doi.org/10.1029/98RG00716.

Kawasaki, I., Tanimoto, T., 1981. Radiation patterns of body waves due to the seismic dislocation occurring in an anisotropic source medium. Bull. Seismol. Soc. Am. 71, 37–50.

Keller, G.V., Grose, L.T., Murray, J.C., Skokan, C.K., 1979. Results of an experimental drill hole at the summit of Kilauea volcano, Hawaii. J. Volcanol. Geotherm. Res. 5, 345–385. https://doi.org/10.1016/0377-0273(79)90024-6.

Krischer, L., Mengies, T., Barsch, R., Beyreuther, M., Lecocq, T., Caudron, C., Wassermann, J., 2015. ObsPy: a bridge for seismology into the scientific Python ecosystem. Comput. Sci. Discov. 8. https://doi.org/10.1088/1749-4699/8/1/014003.

Kumagai, H., 2001. Very-long-period seismic signals and caldera formation at Miyake Island, Japan. Science 293, 687–690. https://doi.org/10.1126/science.1062136.

Kumagai, H., Chouet, B., Dawson, P.B., 2005. Source process of a long-period event at Kilauea volcano, Hawaii. Geophys. J. Int. 161, 243–254. https://doi.org/10.1111/j.1365-246X.2005.02502.x.

Laske, G., Masters, G., Ma, Z., Pasyanos, M.E., 2013. Update on CRUST1.0: a 1-degree global model of Earth's crust. In: Geophys. Res. Abstracts, vol. 15. Abstract EGU2013-2658.

Massé, R.P., 1981. Review of seismic source models for underground nuclear explosions. Bull. Seismol. Soc. Am. 71, 1249–1268.

Matoza, R.S., Chouet, B.A., Dawson, P.B., Shearer, P.M., Haney, M.M., Waite, G.P., Moran, S.C., Mikesell, T.D., 2015. Source mechanism of small long-period events at Mount St. Helens in July 2005 using template matching, phase-weighted stacking, and full-waveform inversion. J. Geophys. Res., Solid Earth 120, 6351–6364. https://doi.org/10.1002/2015JB012279.

Matoza, R.S., Okubo, P.G., Shearer, P.M., 2021. Comprehensive high-precision relocation of seismicity on the Island of Hawai'i 1986-2018. Earth Space Sci. 8. https://doi.org/10.1029/2020EA001253.

Matoza, R.S., Shearer, P.M., Lin, G., Wolfe, C.J., Okubo, P.G., 2013. Systematic relocation of seismicity on Hawaii Island from 1992 to 2009 using waveform cross correlation and cluster analysis. J. Geophys. Res. 118, 2275–2288. https://doi.org/10.1002/jgrb.50189.

Michon, L., Massin, F., Famin, V., Ferrazzini, V., Roult, G., 2011. Basaltic calderas: collapse dynamics, edifice deformation, and variations of magma withdrawal. J. Geophys. Res. 116, B03209. https://doi.org/10.1029/2010JB007636.

Michon, L., Staudacher, T., Ferrazzini, V., Bachèlery, P., Marti, J., 2007. April 2007 collapse of Piton de la Fournaise: a new example of caldera formation. Geophys. Res. Lett. 34, L21301. https://doi.org/10.1029/2007GL031248.

Michon, L., Villeneuve, N., Catry, T., Merle, O., 2009. How summit calderas collapse on basaltic volcanoes: new insights from the April 2007 caldera collapse of Piton de la Fournaise volcano. J. Volcanol. Geotherm. Res. 184, 138–151. https://doi.org/10.1016/j.jvolgeores.2008.11.003.

Minson, S.E., Dreger, D.S., Bürgmann, R., Kanamori, H., Larson, K.M., 2007. Seismically and geodetically determined nondouble-couple source mechanisms from the 2000 Miyakejima volcanic earthquake swarm. J. Geophys. Res. 112. https://doi.org/10.1029/2006JB004847.

Neal, C.A., Brantley, S.R., Antolik, L., Babb, J.L., Burgess, M., Calles, K., Cappos, M., Chang, J.C., Conway, S., Desmither, L., Dotray, P., Elias, T., Fukunaga, P., Fuke, S., Johanson, I.A., Kamibayashi, K., Kauahikaua, J., Lee, R.L., Pekalib, S., Miklius, A., Million, W., Moniz, C.J., Nadeau, P.A., Okubo, P.G., Parcheta, C., Patrick, M.R., Shiro, B., Swanson, D.A., Tollett, W., Trusdell, F., Younger, E.F., Zoeller, M.H., Montgomery-Brown, E.K., Anderson, K.R., Pol, M.P., Ball, J.L., Bard, J., Coombs, M., Dietterich, H.R., Kern, C., Thelen, W.A., Cervelli, P.F., Orr, T., Houghton, B.F., Gansecki, C., Hazlett, R., Lundgren, P., Diefenbach, A.K., Lerner, A.H., Waite, G., Kelly, P., Clor, L., Werner, C., Mulliken, K., Fisher, G., Damby, D., 2019. The 2018 rift eruption and summit collapse of Kīlauea Volcano. Science 363, 367–374. https://doi.org/10.1126/science.aav7046.

Okubo, P., Nakata, J.S., 2003. Tectonic pulses during Kīlauea's current long-term eruption. In: Heliker, C., Swanson, D.A., Takahashi, T.J. (Eds.), The Pu'u 'Ō'ō-Kūpaianaha Eruption of Kīlauea Volcano, Hawai'i: The First 20 Years. U.S. Geol. Survey, Washington, D.C., pp. 173–186. Professional Paper 1676.

Patrick, M.R., Dietterich, H.R., Lyons, J.J., Diefenbach, A.K., Parcheta, C., Anderson, K.R., Namiki, A., Sumita, I., Shiro, B., Kauahikaua, J.P., 2019. Cyclic lava effusion during the 2018 eruption of Kīlauea Volcano. Science 366, eaay9070. https://doi.org/10.1126/science.aay9070.

Ruch, J., Acocella, V., Geshi, N., Nobile, A., Corbi, F., 2012. Kinematic analysis of vertical collapse on volcanoes using experimental models time series. J. Geophys. Res., Solid Earth 117, B07301. https://doi.org/10.1029/2012JB009229.

Scandone, R., 1990. Chaotic collapse of calderas. J. Volcanol. Geotherm. Res. 42, 285–302. https://doi.org/10.1016/0377-0273(90)90005-Z.

Schultz, R.A., 1993. Brittle strength of basaltic rock masses with applications to Venus. J. Geophys. Res., Planets 98, 10883–10895. https://doi.org/10.1029/93JE00691.

Segall, P., Anderson, K.R., Johanson, I., Miklius, A., 2019. Mechanics of inflationary deformation during caldera collapse: evidence from the 2018 Kīlauea eruption. Geophys. Res. Lett. 46, 11782–11789. https://doi.org/10.1029/2019GL084689.

Shelly, D.R., Thelen, W.A., 2019. Anatomy of a caldera collapse: Kīlauea 2018 summit seismicity sequence in high resolution. Geophys. Res. Lett. 46, 14395–14403. https://doi.org/10.1029/2019GL085636.

Shuler, A., Ekström, G., Nettles, M., 2013a. Physical mechanisms for vertical-CLVD earthquakes at active volcanoes. J. Geophys. Res. 118, 1569–1586. https://doi.org/10.1002/jgrb.50131.

Shuler, A., Nettles, M., Ekström, G., 2013b. Global observation of vertical-CLVD earthquakes at active volcanoes. J. Geophys. Res. 118, 1–27. https://doi.org/10.1029/2012JB009721.

Silwal, V., Tape, C., 2016. Seismic moment tensors and estimated uncertainties in southern Alaska. J. Geophys. Res., Solid Earth 121, 2772–2797. https://doi.org/10.1002/2015JB012588.

Simkin, T., Howard, K.A., 1970. Caldera collapse in the Galápagos Islands, 1968. Science 169, 429–437. https://doi.org/10.1126/science.169.3944.429.

Tape, W., Tape, C., 2013. The classical model for moment tensors. Geophys. J. Int. 195, 1701–1720. https://doi.org/10.1093/gji/ggt302.

Tape, W., Tape, C., 2019. The eigenvalue lune as a window on moment tensors. Geophys. J. Int. 216, 19–33. https://doi.org/10.1093/gji/ggy373.

Trugman, D.T., Shearer, P.M., 2017. GrowClust: a hierarchical clustering algorithm for relative earthquake relocation, with application to the Spanish Springs and Sheldon, Nevada, earthquake sequences. Seismol. Res. Lett. 88, 379–391. https://doi.org/10.1785/0220160188.

Zablocki, C.J., Tilling, R.I., Peterson, D.W., Christiansen, R.L., Keller, G.V., Murray, J.C., 1974. A deep research drill hole at the summit of an active volcano, Kilauea, Hawaii. Geophys. Res. Lett. 1, 323–326. https://doi.org/10.1029/GL001i007p00323.

Zhu, L., Rivera, L.A., 2002. A note on the dynamic and static displacements from a point source in multilayered media. Geophys. J. Int. 148, 619–627. https://doi.org/10.1046/j.1365-246X.2002.01610.x.